Title

High-resolution simulation of free-surface flow and tracer retention over streambeds with ripples

Authors

Broecker, Tabea
Elsesser, Waldemar
Teuber, Katharina
et al.

Publication Date

2018

DOI

10.1016/j.limno.2017.06.005

Peer reviewed

High-resolution simulation of free-surface flow and tracer retention over streambeds with ripples

Tabea Broecker[a] Waldemar Elsesser[a] Katharina Teuber[a] Ilhan Özgen[a] Gunnar Nützmann[bc] Reinhard Hinkelmann[a]

Abstract

This study presents a novel high-resolution simulation of free-surface flow and tracer retention over a streambed with ripples based on varying ripple morphologies, surface hydraulics and the transport of a tracer pulse from surface water to surface dead zone. For the simulations, the computational fluid dynamics (CFD) model OpenFOAM was used to solve the three-dimensional Navier-Stokes equations in combination with an implemented transport equation. Pressure gradients at the streambed were used to account for hyporheic exchange, assuming water flow from high pressure zones to low pressure zones. Flow velocities, ripple sizes and spacing showed to significantly affect these pressure gradients, but also the transport of a passive tracer at the streambed, which was not investigated so far. Due to the velocity field, large parts of the tracer mass were transported alongside the main stream above the ripples. Tracer mass reaching the space between the ripples was temporarily retained due to low velocities and recirculations. It was shown that the retention is depending on the ripple size and space between the ripples as well as on the flow velocity. Decreasing ripple sizes and higher flow velocities lead to a smaller tracer retention. Furthermore we showed that the ripple length to height ratio controls the generation of recirculation zones which affect the residence time of the tracer significantly. Ripple spacing leads to temporarily higher tracer concentration at the streambed, but smaller tracer retention. We conclude that the impact of the streambed morphology on the hydraulics in combination with tracer retention should be addressed for a comprehensive understanding of compound movement, exchange and transformation within the hyporheic zone.

Keywords: Numerical modeling, Ripples, Hyporheic exchange, Tracer retention, Tracer transport, Turbulence

1. Introduction

The hyporheic zone is the transition zone between aquifer and river (Buss et al., 2009). Processes within this zone are essential for the water balance, the movement of water and the substances transported and transformed therein. Consequently, the hyporheic zone has a strong influence on the health of fluvial systems e.g. through biogeochemical processes (Bardini et al., 2012, Dahm et al., 1998, Harvey and Fuller, 1998). These exchange processes occur at a wide range of spatial scales (Stonedahl et al., 2010) reaching from small scale riverbed topographies like ripples and dunes (Elliott and Brooks, 1997, Packman and Brooks, 2001, Boano et al., 2007, Cardenas and Wilson, 2007b) to larger geomorphological features like

meander bends (Boano et al., 2006, Revelli et al., 2008, Cardenas, 2008). A driving force for the exchange are pressure differences along the streambed (Buffington and Tonina, 2009, Thibodeaux and Boyle, 1987, Elliott and Brooks, 1997).

Considering the complexity of turbulent flow and accompanied hyporheic exchange, it is quite challenging to perform adequate flume experiments or field studies of the groundwater-surface water interaction. Therefore computational fluid dynamics (CFD) models are often a good alternative. CFD models offer high-resolution information on flow field characteristics which help to get a better insight into complex flow and transport processes. Especially three-dimensional models have the potential to consider the complex mechanisms of flow dynamics in all three directions (Lane et al., 2002, Chen et al., 2015, Shen and Diplas, 2008, Trauth et al., 2013, Trauth et al., 2015, Tonina and Buffington, 2007, Tonina and Buffington, 2009b), whereas vertically-averaged one- and two-dimensional hydraulic models are based on the hydrostatic pressure assumption. Therefore, it is not possible to determine vertical velocities using the latter models (Hinkelmann, 2005). Especially for the examination of turbulence, which also can cause hyporheic exchange (Tonina and Buffington, 2009a) and affect the flow of substances, the investigation of all three directions is important. Here, one-, two- or multiphase models can be applied. According to Stoesser et al. (2008) a shear-free symmetric boundary condition assumption suffices for high water levels as long as the Froude number is not bigger than 0.8, whereas for relatively shallow turbulent flow over streambed structures a two-phase model is appropriate (Yue et al., 2005).

A large number of publications have reported numerical simulations of flow, transport and reaction processes within the hyporheic zone (Trauth et al., 2014, Cardenas et al., 2008, Bardini et al., 2012). However, according to the author's knowledge, only the flow of surface water into the ground, not the transport of a tracer pulse from surface water into surface dead zones and the ground was simulated with numerical models. Furthermore, previous studies investigating the influence of amplitudes and wavelengths of dune-like structures on the hyporheic exchange did not include structure spacing.

This study aims to improve the understanding of flow and transport dynamics of a passive tracer in surface water with a focus on the processes occurring between the ripples using a three-dimensional computational fluid dynamics (CFD) model. High resolution simulations are carried out to analyse pressure and velocity distributions. Several simulations are investigated using a one phase as well as a two-phase flow and transport model. In contrast to previous studies, where hyporheic exchange was quantified or the residence times in the hyporheic zone were presented, this study investigates pressure fluctuation and the generation of recirculation zones between ripples which cause a tracer retention between the ripples and thus has impact on hyporheic exchange. We hypothesize that ripple dimensions, lengths and spacing as well as varying flow rates have a clear impact on the

flow dynamics as well as on tracer spreading and retention at the river bed which in turn will affect the hyporheic exchange.

2. Governing equations and numerical method

The OpenSource CFD software OpenFOAM (Open Field Operation and Manipulation) version 2.4.0 is used to simulate flow processes over a rippled streambed. As in most hydraulic engineering applications using OpenFOAM, the interFoam-solver is applied (Schulze and Thorenz, 2014). interFoam is a multiphase solver for immiscible fluids that solves the three-dimensional Navier-Stokes equations using the Finite-Volume-Method in space and the Finite-Differences-Method in time. The OpenFOAM toolbox allows parallel computations on a theoretically unlimited number of processor cores and enables the user to take full advantage of the computer hardware. Regarding the simulation of water channelswith complex stream bed morphologies, flow and pressure distributions can most realistically be depicted with the full Navier-Stokes equations (Cardenas and Wilson, 2007b, Tonina and Buffington, 2009a, Janssen et al., 2012). A common assumption for free surface flow is that it may be considered to be incompressible. This can be estimated if the Mach number (the ratio of the flow velocity to the sound velocity) is below 0.3 (Young et al., 2010). For incompressible flow, the conservation of mass (Eq. (1)) and momentum (Eq. (2)) are written as:

$$(1)\nabla v=0$$

$$(2)\partial\rho v\partial t+v\nabla\rho v=-\nabla p+\mu phys+\mu turb\Delta v+\rho g$$

where ρ represents the density of the fluids, v is the flow velocity, t is time, ρ is pressure, μ_{phys} and μ_{turb} are the physical and turbulent dynamic viscosity, respectively, and g is the gravitational acceleration. The interface is captured by a Volume-of-Fluid-Method (Hirt and Nichols, 1981). A single variable value per element, the indicator fraction α, expresses the proportion of the fluids. It considers the fluids to be a single multiphase fluid with properties (dynamic viscosity and density) that are weighted according to the fractions of each fluid (Eqs. (3) and (4)). The indicator fraction α varies between 0 (air) and 1 (water). The movement of the water-air interface is described by a convective transport equation (Eq. (5)).

$$(3)\mu=\mu water\alpha+\mu air1-\alpha$$

$$(4)\rho=\rho water\alpha+\rho air1-\alpha$$

$$(5)\partial\alpha\partial t+\nabla\alpha v=0$$

For the pressure-velocity coupling the PIMPLE algorithm is used. It is a combination of the widely used SIMPLE and PISO algorithms which uses the outer-correction tool of SIMPLE and the inner-corrector loop of PISO to gain a more robust coupling (Rodrigues et al., 2011). Turbulent features can be resolved directly with a very fine mesh or – like in most cases – are partially or completely modeled. In the following, a large eddy simulation (LES) model is applied to predict turbulent flows. LES turbulence models simulate eddies

of a certain size directly. Only small turbulent structures are separated by a low-pass filter and subsequently treated with an algebraic model. In this case, the Smagorinsky subgrid scale model is used with a van Driest damping function. The purpose of the van Driest damping is to reduce the eddy viscosity in the near-wall region allowing to reproduce the characteristics of direct numerical simulations at the near-wall region which solve the three-dimensional Navier-Stokes equations for all eddies directly.

Since the interFoam-solver does not provide an application for the transport of a passive tracer, an advection-diffusion equation was implemented into the interFoam-solver (Eq. (6)). This additional implementation allows to investigate the transport of a passive tracer with a concentration C through the channel. Regarding the diffusivity, the user can define the physical diffusivity coefficient D_{phys} as well as the turbulent Schmidt number Sc_t. According to Eq. (7) the turbulent diffusivity coefficient D_{turb} will be calculated.

(6)∂C∂t+∇Cv+∇Dphys+Dturb∇C=0

(7)Dturb=μturb/ρSct

3. Validation

In order to verify the numerical results concerning the hydraulics, the model was validated based on two laboratory experiments which are described in the following.

Almeida et al. (1990) performed and presented a flume experiment with a single ripple on the bottom of a channel (see Fig. 1a). This experiment was used to ensure a reliable physical behavior of the developed model – especially concerning velocity distributionsaround ripples. Flow velocities in two dimensions over a polynomial-shaped obstacle were measured using a Laser-Doppler Velocimeter up to 2 mm from the surface of the ripple and the bottom of the channel. The top of the channel consisted of a wall, while the whole channel was filled with water. The mean velocity at the inlet was 2.147 m/s.

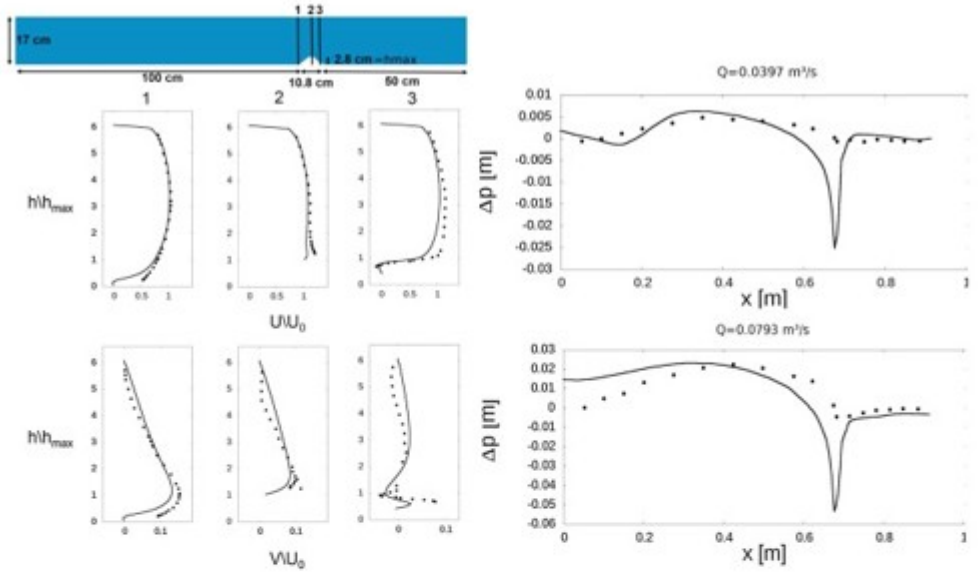

(a) Velocity profiles in a flume with a single ripple (b) Pressure difference profiles along triangular bedform

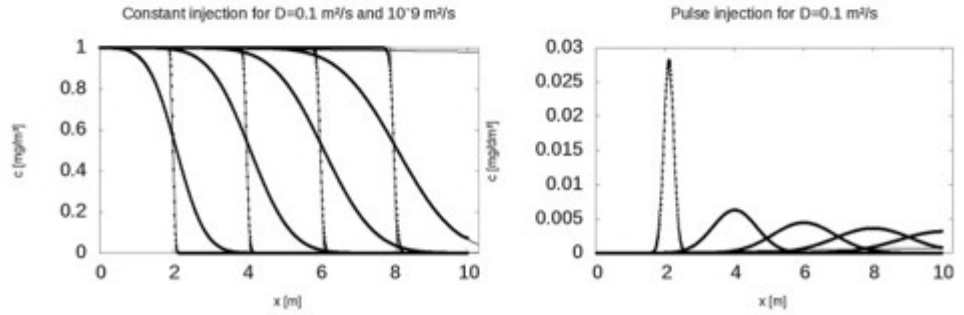

(c) Tracer breakthrough curves

Fig. 1. Comparison of measured or with analytical solutions calculated data (points) with simulated data (lines).

The boundary conditions were adjusted slightly, since only one phase instead of two-phases as well as a fixed wall on the top instead of an atmospheric boundary had to be imposed according to the experimental setup. Furthermore velocities were only measured in two dimensions. Therefore a two-dimensional model was adequate for this validation. The model entry was extended in front of the hill to achieve fully developed velocity profiles. Since a velocity function was set as inlet boundary, an entrance length of 1 m in front of the hill was sufficient to receive a fully developed flow. Velocity profiles of the simulations in *x*- and *y*-direction at six different locations were compared to the measurements. The geometry of the model is presented in Fig. 1a (top). Various turbulence models (three Reynolds Averaged Navier Stokes turbulence models and a Large-Eddy-Simulation) are applied to investigate the turbulence. Comparing the measured data of the experiments with the simulation datausing different turbulence models, the

LES turbulence model indicated the best agreement. Moreover, Fig. 1a shows the resulting velocities in *x*- and *y*-direction for the simulation with the LES model and the experimental data at three locations. A good agreement with the measured data was observed.

Next to the measurements by Almeida et al. (1990), flume data by Fehlman (1985) were used to validate the model. Compared to Almeida et al. (1990), the data by Fehlman (1985)were used to ensure reliable pressure distribution of a three-dimensional, two-phase model. Fehlman investigated flow over beds with triangular ripples for twelve runs with discharges between 0.021 m^3/s and 0.140 m^3/s and examined pressure variations (see Fig. 1b).

The geometry of Fehlman's flume including the triangular bed forms was discretized with the help of three-dimensional meshes. The results of the simulations were compared with experimental data of two different discharges (Run 4 and Run 10) of Fehlman's examinations. Fig. 1b shows a comparison of measured and simulated differences in pressure heads between the bed form surface and the crest of the ripple for a discharge of 0.0397 m^3/s and of 0.0793 m^3/s.

In this context it should be emphasized, that there were no pressure taps at the crest and consequently the pressure was linearly interpolated. Trauth et al. (2013) and Cardenas and Wilson (2007) used the same experiment for the validation and pointed out that the crest is a singularity with an adverse pressure gradient which is challenging to capture numerically or experimentally. Therefore it is very difficult to compare the measured and the simulated results. To improve the comparability, pressure heads for a point downstream of the crest are subtracted instead of the value directly at the crest. Despite this singularity at the crest, which was also depicted by Cardenas and Wilson (2007) and Trauth et al. (2013), the simulated variations along the bed forms were in good agreement with the experiments.

For the validation of the transport, four analytical one-dimensional solutions after Kinzelbach (1992) were used for a constant tracer injection as well as for a tracer pulse for two different diffusion values: $D_{phys} = 10^{-9}$ m^2/s (neglecting turbulent diffusion) and $D_{phys} = 0.1$ m^2/s (strong turbulent diffusion). We are aware that the value for the turbulent diffusion is very high, however we thus could check the implementation of the diffusion term. A good agreement was achieved between the simulations and the analytical solutions as it can be seen in Fig. 1c.

In summary, the model concept was tested against data of two flume experiments as well as against analytical solutions. Different parameters were examined and the simulations demonstrate that the surface model shows good accuracy concerning the pressure head distributions, the calculated velocities and the tracer concentrations.

4. Simulations of flow and transport over streambeds with ripples

Based on the successful validation of the model, flow velocities, water elevations and pressure distributions as well as the transport of a passive tracer pulse were investigated for differing ripple geometries and flow rates as shown in Fig. 2a. Firstly, the reference case will be presented. Based on these results, the influence of above-mentioned cases are analyzed.

Case	1	2	3	4	5	6	7
Ripple height [cm]	5.6	1.4	11.2	5.6	5.6	5.6	5.6
Ripple length [cm]	20	5	40	40	20	20	20
Ripple distance [cm]	0	0	0	0	20	0-56	0
Flow rate [m^3/s]	0.5	0.5	0.5	0.5	0.5	0.5	0.25
Schmidt number [-]	1 & 0.5	1	1	1	1	1	1

(a)

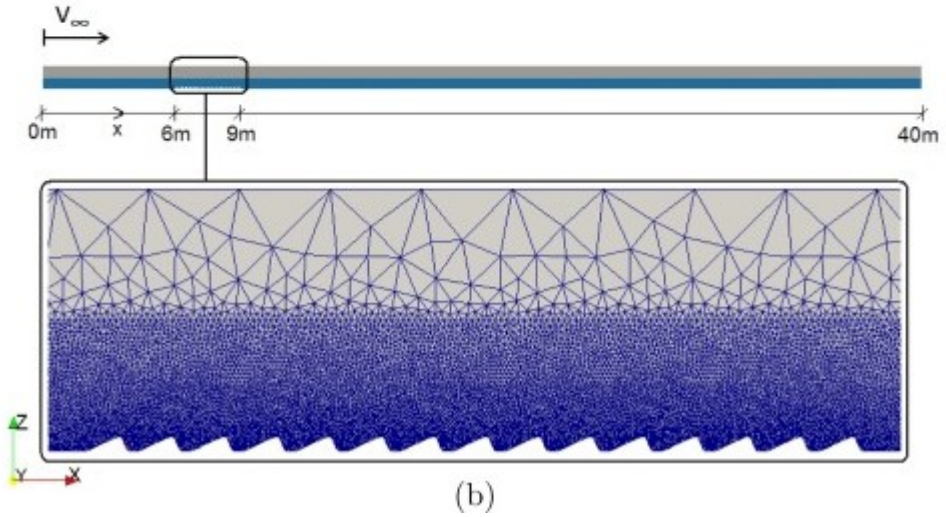

(b)

Fig. 2. Simulation cases (a), model geometry and mesh for the reference case (b).

4.1. Geometry and mesh

Fig. 2b shows the geometry of the system and the bathymetry with the initial water level for the reference case. For all simulations, the domain is a prismatic rectangular channel with a height and width of 1 m and a length of 40 m. After an inflow area of 6 m, a field with varying number of ripples (7 to 64) with differing geometries and distances is introduced. The length of this field comprises approximately 3 m. The length of the whole system was set to guarantee an undisturbed outlet in order to set proper boundary

conditions – especially for larger ripple heights which affect the water surface.

The ripples show a small gradient at the upstream face, and a steep gradient at the downstream face. For different simulation runs, the height is varied from 0.014 m to 0.112 m, the length is varied between 0.05 m and 0.4 m and the distance between the ripples is varied from 0 m to 0.56 m. The mesh in the nearfield of the ripples is refined as shown exemplarily in Fig. 2b. Due to the curved profile in the *x*-*z*-plane, unstructured elements were chosen. The elements were extruded with 10 layers in the *y*-direction to produce prismatic volumes. 6 three-dimensional meshes with up to $1.27 \cdot 10^{6}$ cells were created. Fixed bed forms were assumed for all cases, which means that no sediment transport is examined for this study. Since the air-phase as well as the outflow are not of interest for this study, larger element sizes were chosen for these areas. The minimum cell area in the *x*-*z*-plane amounts to $1.75 \cdot 10^{-5}$ m (located at the rippled streambed) and to the maximum of 0.04 m (within the air-phase) for the reference case. All cases show similar mesh conditions.

4.2. Initial and boundary conditions

The boundary conditions are constant over time to represent steady state flow. An initial water depth (see Fig. 2b) as well as an initial flow velocity are specified to achieve the steady state faster. The inlet is divided into two fractions. In the lower fraction only water enters the domain, in the upper half only air flow is possible. The discharge of the water that enters the domain is fixed. For the air fraction at the inlet as well as on the upper boundary atmospheric pressure is defined. At the outlet a mean velocity for the water phase is set. The velocity profile as well as the water depth are not fixed due to zero gradient boundary conditions at the outlet. At the streambed the velocity is set to 0 m/s. For the transport simulations zero concentration is assumed at the inlet as well as at the upper boundary, the rest is set to a zero gradient condition. Starting from steady state, a passive tracer with a density of 1 kg/m^3 is placed into the water phase as initial condition nearby the inlet with a volume of 0.5 m × 0.5 m × 1 m in the *x*-, *z*- and *y*-direction. For the turbulent diffusivity, a turbulent Schmidt number of 1 is set. The physical diffusivity coefficient is 10^{-9} m^2/s. All boundaries in the third dimensions contain slip conditions. Thereby normal components and the gradient of tangential components are set to zero. Consequently the water is able to pass and no influence through lateral walls is given.

4.3. Reference case

For the first case the inlet discharge is set to 0.5 m^3/s, the initial water depth is set to 0.5 m. Hence, the inlet velocity is 1 m/s. The density of the water is 998.2 kg/m^3, the density of the air 1.2 kg/m^3, the physical kinematic viscosity of the water is 10^{-6} m^2/s and the physical kinematic viscosity of the air is $15.3 \cdot 10^{-6}$ m^2/s. Each ripple has a length of 0.2 m, a height of 0.056 m (see

Fig. 2a). Since a semi-implicit time-difference scheme is imposed for all simulations, a time step of 0.05 s is sufficient.

An one-phase as well as a two-phase model were investigated for the reference case. A comparison of the results indicated that the application of a two-phase model is important to depict water level fluctuations which influence the pressure distribution in the domain. These pressure distributions are important for the exchange of surface water with groundwater and should therefore be determined as precisely as possible. Due to the rippled streambed the water surface raises slightly in front of the ripples from $z = 0.5$ m to $z = 0.508$ m. At the area of the ripples the water surfaces decreases down to $z = 0.483$ m due to subcritical flow(Froude number of 0.45) over an elevated ground (see Jirka (2007)). Since a relatively shallow turbulent flow (e.g. a small river or creek) is considered, the structure is better represented by a two-phase model.

Fig. 3a shows the velocity distribution in x- and z-direction at the crest height for the first ten ripples as well as the velocity in x-direction for the rippled streambed (Fig. 3b). The flow accelerates at the first ripple up to 1.49 m/s. The maximum velocity occurs near the crest at the stoss side. Compared to the following ripples, the flow is particularly accelerated at the first ripple. Behind the crest the flow velocity is very low, but accelerates again at the next ripple crest. The flow velocity at the streambed changes from positive to negative values up to -0.525 m/s. Negative velocities indicate the separation zone of the flow downstream of the crest. Starting with the second ripple, the velocity distribution is periodical for each ripple: small velocities between the ripples, flow acceleration at the crest.

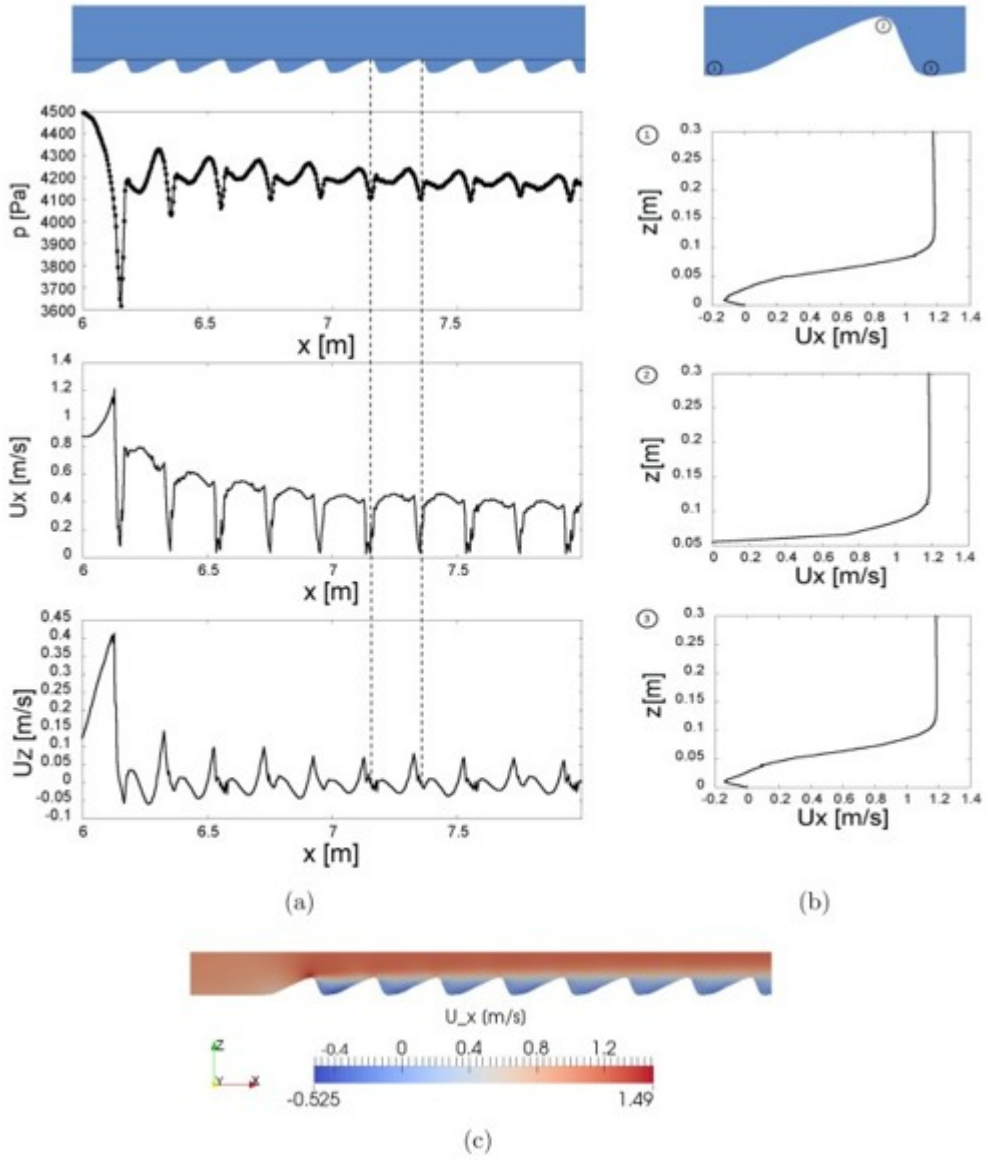

Fig. 3. Pressure and velocity distribution for the reference case for the whole ripple domain (a), velocity profile at a ripple in the middle of the rippled bedform (sixth ripple) (b), velocity distribution in the domain (c).

In the *z*-direction, the flow accelerates from 0 m/s at the inlet up to 0.44 m/s upstream of the first ripple. Here, the three-dimensional Navier-Stokes model shows considerable differences in the third dimension which also will have a strong impact on the exchange with the underlying hyporheic zone. At the ripple crest the flow decelerates and reaccelerates at the ripple lee. At the next ripple stoss the flow decelerates and turns initially negative. A constant variation pattern of negative and positive flow velocities in *z*-direction can be recognized starting with the second ripple. A recirculation zone with a three-dimensional structure can be observed behind each ripple.

Fig. 3b shows the velocity profiles at a ripple located in the middle of the rippled bedform(the sixth ripple) at three different points. Each profile starts

with 0 at the wall. Up- and downstream of the ripple negative velocities are determined. The minimum velocity amounts −0.12 m/s at point 1 and −0.13 m/s at point 3. At half of the ripple height, the velocity turns positive. On top of each crest the flow accelerates compared to the mean inflow velocity of 1 m/s with a maximum of 1.19 m/s. Comparing the velocity of the rippled bedform with the flow field at the flat streambed, a faster flow can be observed above the ripples, whereas a zone of small velocities appears between the ripples.

Simulated pressure distributions near the streambed are of interest for predicting the hyporheic flow since water flows from high pressure zones to low pressure regions. The solver interFoam solves the pressure term p _ rgh which is defined as p _ rgh = $p - \rho g z$ with the hydrostatic pressure p and z as coordinate vector. p _ rgh is used – rather than p – 'to avoid deficiencies in the handling of the pressure force/buoyant force balance on non-orthogonal and distorted meshes' (see OpenFOAM Greenshields (2010)). In front of each ripple the pressure increases (see Fig. 3a). At the crest an adverse pressure gradient can be observed with a maximum pressure difference of 1060 Pa – corresponding to a water level of 0.106 m. The highest pressure difference is determined at the first crest.

Fig. 4 shows the tracer distribution at the beginning, after 3 s, 6 s, 7 s and after 10 s for the reference case. Next to the streambed the tracer is transported slower, compared to the mainstream, due to smaller velocities near the bottom. Most of the tracer is transported advectively with a velocity around 1 m/s, which is the mean velocity. After 6 s the tracer reaches the first ripples. The tracer is firstly accumulated in front of the first ripple. Due to the velocity profile at the ripple stoss, the tracer can flow across the first ripple. The advective transport of the tracer is now concentrated on the flow above the ripples. The main tracer concentration passes the rippled section after less than 9 s.

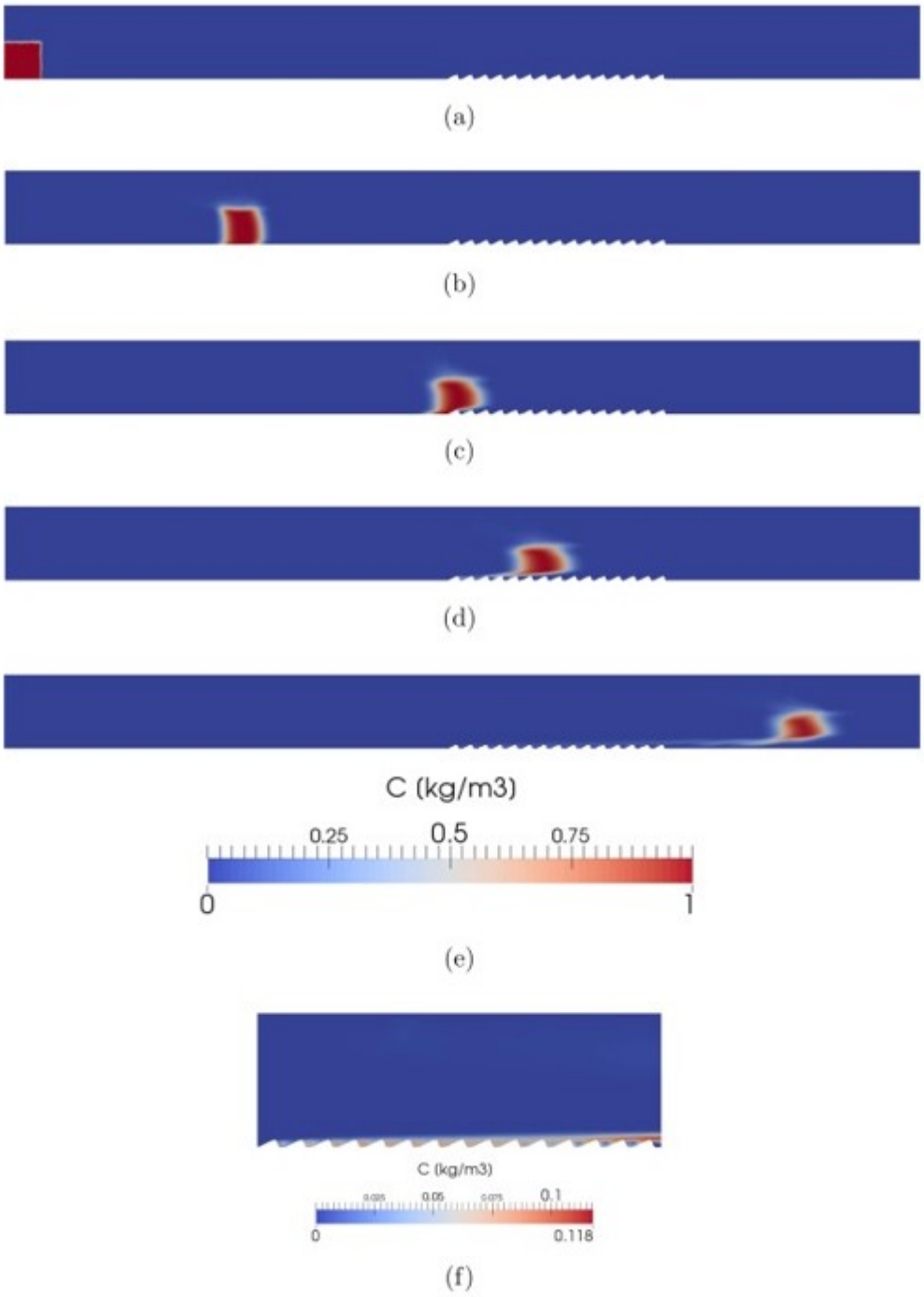

Fig. 4. Tracer distribution at t = 0 s (a), t = 3 s (b), t = 6 s (c), t = 7 s (d), t = 10 s (e) (from section x = 0 m to x = 12 m, top) and for the rippled area (section from x = 6 m to x = 9 m, bottom) at t = 10 s (f) for the reference case.

The simulation indicates that the tracer moves slightly in all directions driven by turbulent diffusion. Considering this fact and the local flow field, the tracer spreads also into the area between the ripples. The tracer shows a relatively long residence time in this area as result of the eddies between the ripples and their inherent small velocities. After 10 s a maximum tracer

concentration of 11.8% of the initial concentration is still determined in the area around the ripples (see Fig. 4f). Maximum tracer concentrations of 5% and of 1% at the rippled streambed are observed after 18.5 s and 39 s at the stoss side of the last ripple. The volume between the ripples can act as a storage volume for tracer which can lead to an increased and temporarily shifted exchange of tracer between surface and groundwater.

For a decreased Schmidt number from 1 to 0.5 the turbulent diffusion increases from maximum $3 * 10^{-7}$ m^2/s to maximum $6 * 10^{-7}$ m^2/s (see Eq. (7)). This leads to less retention, with a maximum tracer concentration of less than 5% already after 14 s and 1% after 31 s (8 s less than for a Schmidt number of 1).

4.4. Variation of ripple dimensions

Next to the reference case two simulations were executed with the same settings like the reference case, only varying the ripple dimensions (see Fig. 2, case 2 and 3): for case 2 the ripple is quartered (length: 0.05 m, height: 0.014 m) and for case 3 it is doubled (length: 0.20 m, height: 0.112 m).

For a ripple height of 0.014 m a maximum velocity of 1.09 m/s and a minimum of −0.334 m/s were observed in the *x*-direction. Thus, an absolute difference of 0.4 m/s (reference case: 1.49 m/s) for positive velocities and 0.191 m/s for negative velocities were determined compared to the reference case with higher ripples (reference case: −0.525 m/s). In the *z*-direction the negative values are 0.048 m/s higher and the positive values 0.154 m/s lower than the reference case with 0.44 m/s. The maximum pressure difference at the streambed amounts to 580 Pa which corresponds to about half of the reference case. Therefore, compared to the reference case, a significantly smaller hyporheic exchange is expected as shown by Cardenas and Wilson (2007). The maximum pressure difference is concentrated at the area of the first ripple. For the following ripples the difference is even smaller. Next to the change of the pressure values, a variance of the location of the minimum pressure is determined: a shift of the minimum pressure from the crest for the reference case to the ripple lee for the simulation with smaller ripples is observed. The slight increase of the water level at the upstream of the first ripple is about 0.007 m and similar to the reference case, though the decrease of only 0.004 m is definitely lower (reference case: 0.017 m). Due to the less accelerated flow in the rippled area (compared to the reference case), the tracer needs more time to pass this area. Therefore, after 10 s the maximum tracer concentration is with 14.6% almost 3% higher than for the reference case (see Fig. 5a). But already after 17 s the maximum tracer concentration is less than 5% and even after 23 s the maximum tracer concentration is less than 1% (16 s difference compared to the reference case). Consequently smaller ripples lead to a less accelerated flow above the ripples, supported by less water level fluctuations, whereby the tracer needs more time to pass the ripples. Between the ripples the tracer is stored for a shorter time. Including the fact,

that the maximum pressure difference is about half of the reference case, a definitely lower tracer exchange with groundwater is expected for smaller ripples.

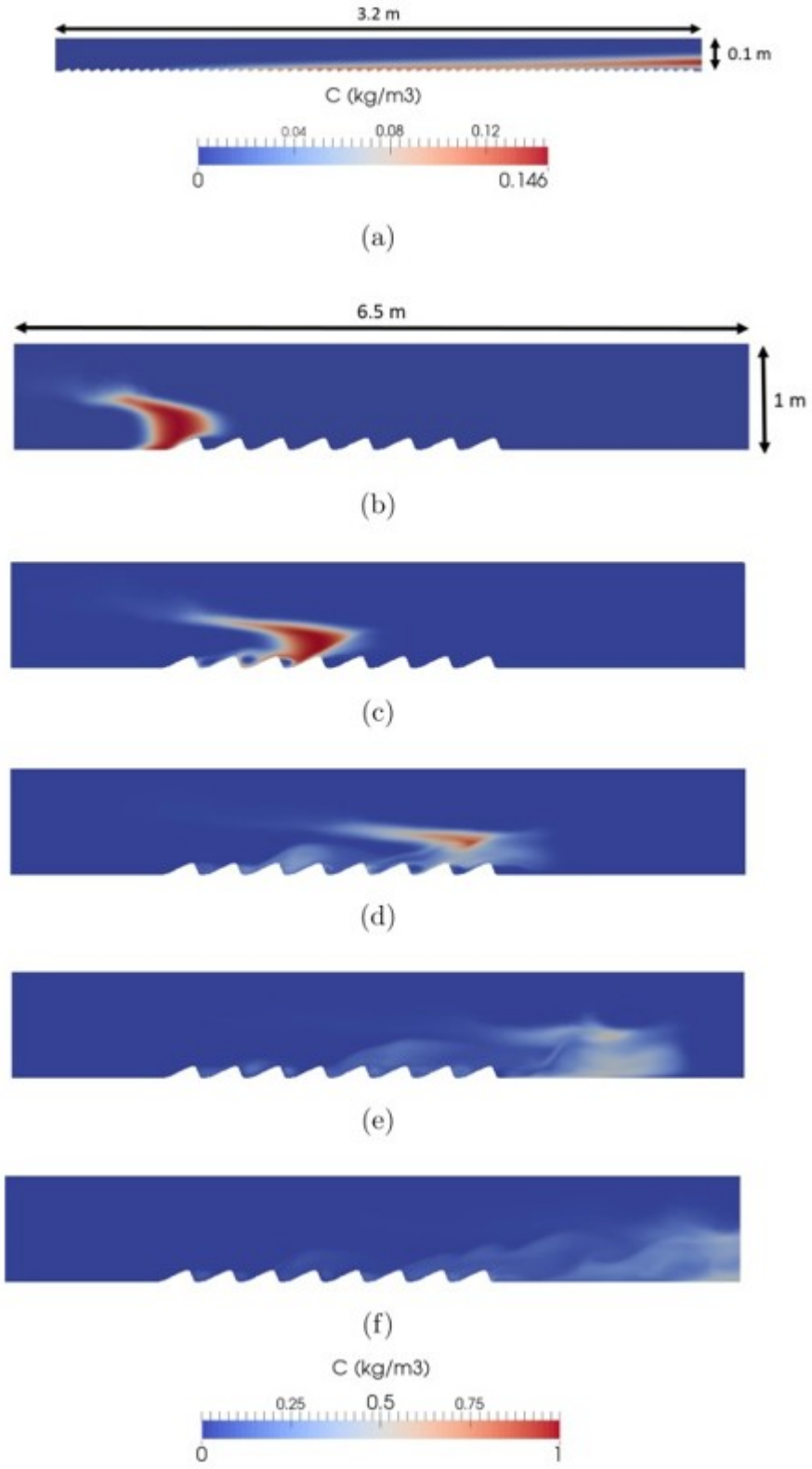

Fig. 5. Tracer distribution for case 2 at t = 10 s (a) and for case 3 at t = 6 s (b), t = 7 s (c), t = 8 s (d), t = 9 s (e), t = 10 s(f).

For the simulation of case 3 (see Fig. 2), waves develop at the water surface. Due to the ripple height the water cross-section is significantly decreased and the flow velocities increased. This leads to a supercritical flow, whereas upstream and downstream of the rippled area subcritical flow is present which results in an undular hydraulic jump (Chanson and Montes, 1995). A comparison of the water level change is therefore difficult. The water level affect also the pressure and velocity distribution at the streambed. Nevertheless small velocities between the ripples and accelerated flow at the crests can be observed over the whole rippled streambed. The maximum velocity in the *x*-direction at the first ripple amounts 1.68 m/s after 1000 s which corresponds to an absolute difference of 0.19 m/s compared to the reference case (reference case: 1.49 m/s). The minimum velocity amounts −1.19 m/s at the same time which corresponds to an absolute difference of 0.665 m/s compared to the reference case (reference case: −0.525 m/s). Thus, the ripple height has a large effect on the velocities in the *x*-direction. In the *z*-direction, the difference between the maximum velocity is 1.08 m/s and more than twice as high as for the reference case (reference case: 0.44 m/s). The minimum velocities are almost three times lower. Due to the disturbed water surface for a ripple height of 0.112 m, the maximum and minimum velocities do not occur periodically for each ripple. The pressure difference at the streambed after 1000 s is with 3220 Pa around three times higher than for the reference case. Next to the low pressure zones at the crests, low pressure zones are recognized also between the ripples.

The undular hydraulic jump has an immense effect on the tracer transport. Fig. 5b–f show the tracer distribution between 6 s and 10 s. Compared to the reference case the transport of the tracer is much more disturbed. There are still some eddies which store the tracer between the ripples, but due to the hydraulic jump the turbulent flow field is definitely higher than for the reference case and leads to a higher spreading of the tracer. After 10 s the maximum tracer concentration at the rippled area amounts to 28.5%, after 15 s to less than 5% and after t=20 s the tracer concentration amounts to less than 1%. This means, that the tracer retention is much lower compared to the reference case and even lower compared to the smaller ripple dimensions of case 2 due to the flow field. However, considering the significantly higher pressure gradient, probably more tracer mass will reach the hyporheic zone compared to the reference case and case 2 even if the retention of tracer between the ripples is smaller.

4.5. Variation of ripple length

For case 4 with a ripple length of 0.4 m (twice as long as the reference ripple, see Fig. 2), the flow is decelerated between the ripples, but no negative velocities occur in the *x*-direction. At the crests, the ripples indicate accelerated flow with a velocity of about 1.5 m/s in the *x*-direction, thus slightly higher velocities as in the reference case with 1.49 m/s. Fig. 6a shows the velocity vectors. In contrast to all other simulated cases no recirculations were determined between the ripples. Regarding a backward

facing-step it is evident, that a limit in the geometry for the descending part of the ripple is exceeded, which causes the flow to not produce eddies because of the smooth geometry. Due to the jam between the ripples, higher pressure is observed just like in front of the first ripple.

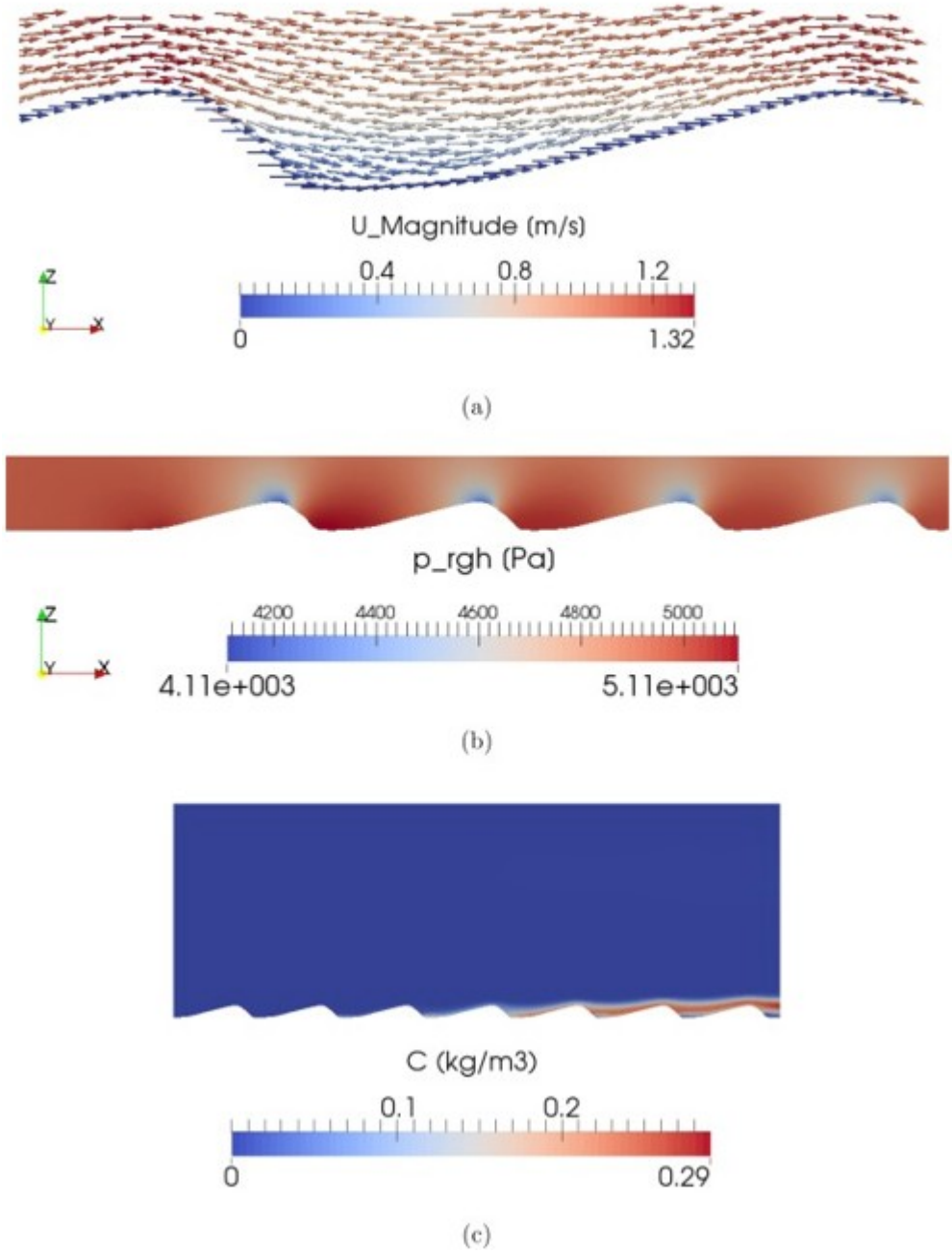

Fig. 6. Velocity vectors (a), pressure distribution (b) and tracer distribution (c) after 10 s for case 4.

The maximum velocity in the *z*-direction is 1.6 times smaller than the maximum velocity in the *z*-direction for the reference case with 0.44 m/s. Unlike the reference case, the velocity at the first crest is similar to the following ripple crests. The same applies for the pressure distribution: the

first ripple shows the same pressure distribution as the following ones (see Fig. 6b) in contrast to all other cases, where the pressure differences between ripple stoss and crest where much higher for the first ripple. The difference of the maximum and the minimum pressure is 1000 Pa and thus similar to the reference case. This leads to the assumption, that a similar hyporheic exchange can be assumed.

Fig. 6c depicts the tracer distribution after 10 s. With a maximum of 29% this case shows a higher concentration than for the reference case at that time. Comparing the whole tracer distribution of both cases, it is obvious, that a pulse tracer injected in the area of streambed with a higher ripple length has a significantly shorter residence time between the ripples. A maximum tracer concentration of 5% is observed after 15 s and a maximum concentration of 1% after 19 s – consequently the shortest residence time of all examined cases. The shorter residence time probably leads to varying hyporheic reactions compared to the other cases. This is most likely based on the flow field which shows no recirculation zones between the ripples retaining the tracer between the ripples (see Fig. 6a).

4.6. Variation of ripple distances

While for the reference case no distance was defined between two ripples, for case 5 a constant distance of 0.2 m, i.e. a horizontal bed, is defined between each ripple pair (see Fig. 2). For the constant ripple distance, the velocities in x-direction were in a similar range as the reference case. The area with small flow velocities has increased due to the distances. Fig. 7a shows that the increased distance leads to a wider recirculation zone in the ripple lee. Due to the LES model, turbulent effects can also be seen in the third dimension. For an increased distance, the maximum velocity in the y-direction is higher.

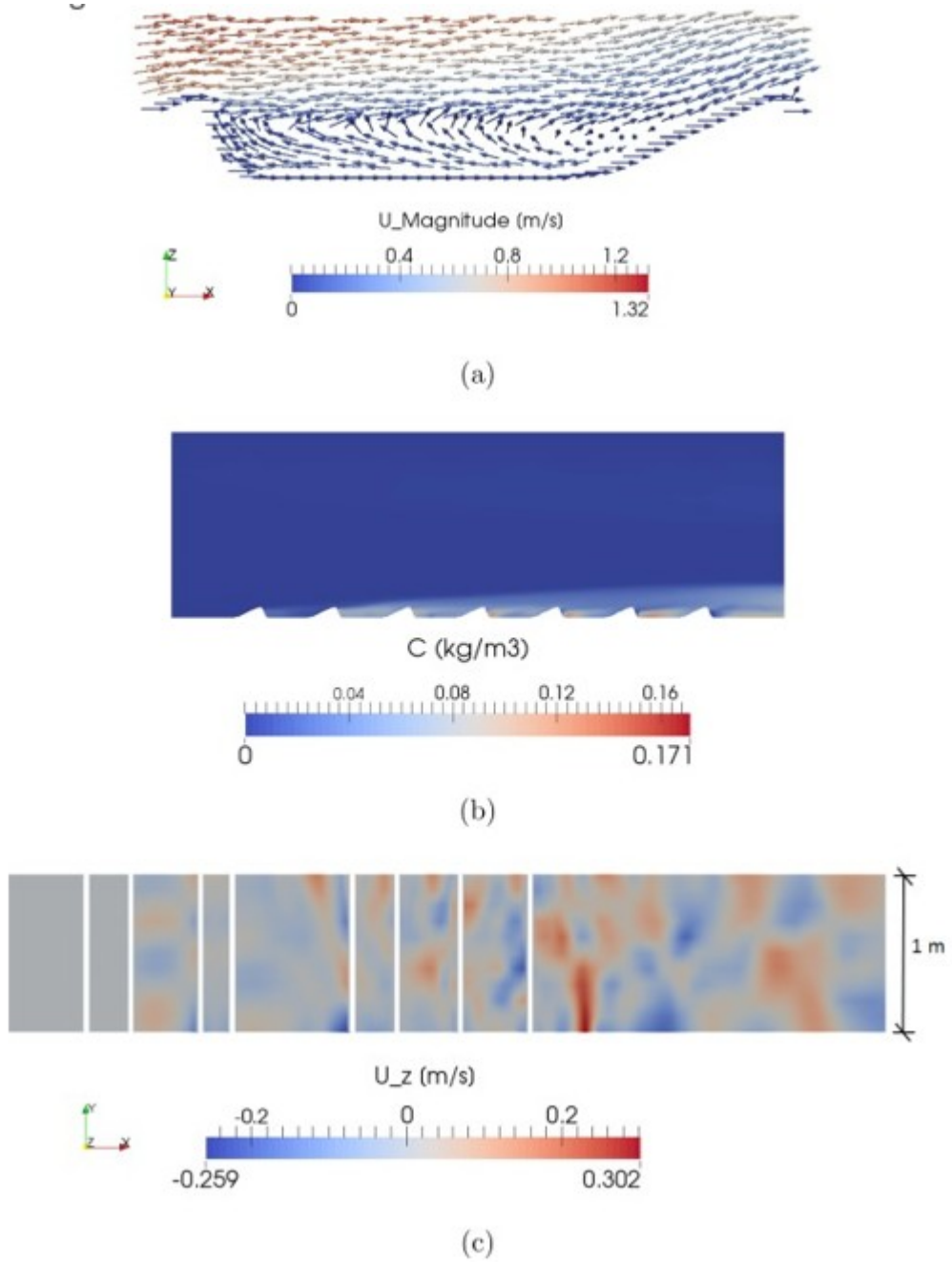

Fig. 7. Velocity vectors (a) and tracer distribution (b) after 10 s for case 5 and velocity in *z*-direction at *z* = 0.05 m for case 6 (c), white lines illustrating the crest (bottom).

Due to the expanded area with small velocities around the ripples, more tracer mass is retained in the rippled area after 10 s compared to the reference case (see Fig. 7b). However it takes only 16 s until the maximum tracer concentration is less than 5% and 28 s for less than 1%. Compared to the reference case, a slightly higher hyporheic exchange flow rate is expected due to higher pressure gradients (pressure difference case 5: 1170 Pa for reference case: 1060 Pa). However, the residence time is smaller for an increasing distance between the ripples.

Following the simulation run with constant distance, the ripple distance is varied between 0 m and 0.56 m for case 6 (see Fig. 2). The previous result is confirmed by the simulation with varying distances, also showing an influence of the flow in the third dimension (see Fig. 7c). The maximum difference between the pressure at the ripple stoss and the crest is 100 Pa higher for the reference case. High pressure fields occur at the first ripple stoss and at ripple stosses downstream of big distances. As for the maximum ripple length, a zone with small pressure between the ripples and the ripple crests was determined. After 10 s the maximum tracer concentration amounts to 13.7%, which is higher than for the reference case. A tracer concentration of less than 1% is observed after 33 s. For case 5 and case 6 a lower retention than for the reference case is noticed. Due to larger distances the tracer mass between the ripples is less protected against the flow.

4.7. Comparison of tracer retention based on ripple geometry

The simulations indicated that the ripple geometry has a significant influence on the retention of a passive tracer in surface dead zones. While the special characteristics of each case were discussed in detail before, in this section a comparison is made between cases 1–6. Fig. 8a shows an overview of the maximum pressure differences across the middle ripple and the maximum concentrations at the middle ripple's toe for each case. In all cases, it was observed that the ripples had a protective function for tracer penetration into the surface dead zone: The maximum tracer concentration that was simulated at the toe of the middle ripple was less than 33% (see Fig. 8a).

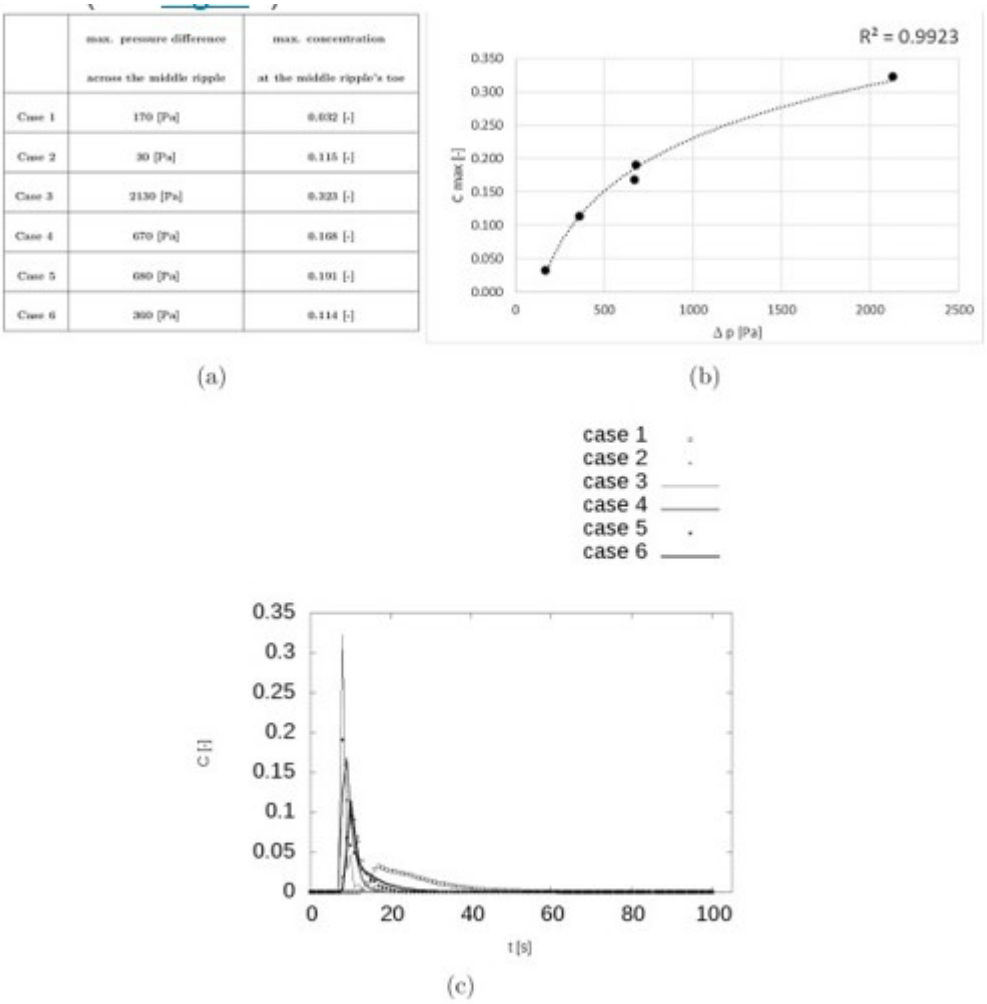

Fig. 8. Maximum pressure differences and tracer concentrations for the ripples in the middle (a and b) and tracer breakthrough curves for the middle ripple's toe (c) for cases 1–6.

Excluding case 2, the maximum tracer concentrations at the middle ripples' toes increase with the maximum pressure differences across the middle ripples, being strongly related by a R^2 of 0.99 for a logarithmic regression function (see Fig. 8b). We excluded case 2, as it the smallest ripple height and the lowest ripple length. Due to the small ripples, low pressure differences were observed. At the same time the small ripples show a smaller protective role towards the streambed. It might be that a certain threshold has not been reached for this case, which leads to higher tracer concentrations despite low pressure differences. Another explanation could be, that due to the less accelerated flow above the ripples, the tracer has more time to enter the area between the ripples and consequently reaches a higher tracer mass.

Whereas the lowest pressure difference was observed for the smallest ripple (case 2), the maximum pressure difference was measured for the highest ripple (case 3), where the maximum tracer concentration was noticed as well. But as it can be seen in Fig. 8c, for this case the retention was

comparatively low. Due to the hydraulic jump the tracer disappeared very fast. Moreover, fluctuations of the tracer concentration were determined. For case 5 a relatively large maximum concentration was detected as well. Due to the absence of eddies, the tracer disappears also very fast. The lowest maximum tracer concentration was determined for the reference case (case 1). Also the maximum pressure difference was relatively low compared to the other cases. In case 1 the duration of the tracer to reach the dead zone between the ripples was longest. However, the retention of the tracer was highest in this case (Fig. 8c). Cases 5 and 6 considered different distances between the ripples (see Fig. 2). Therefore the tracer could enter the space between the ripples easier which lead to higher tracer concentration compared to case 1. However, the tracer was less protected and consequently less retention was observed (Fig. 8c).

4.8. Variation of flow rate

Next to the simulations with a mean flow velocity of 1 m/s, a simulation with a mean inlet velocity of 0.5 m/s has been performed using the geometry and water depth of the reference case (see case 7, Fig. 2). The inlet discharge amounts to 0.25 m^3/s. The velocity distribution seems to be similar to the reference case, but with smaller maximum velocities and larger minimum velocities (max case 1: 1.49 m/s, max case 7: 0.66 m/s, min case 1: −0.525 m/s, min case 7: −0.179 m/s in the *x*-direction). In *z*-direction the range is approximately half of the range of the reference case and consequently ranges around the ratio of the inlet velocities for both cases. The maximum pressure was again determined at the first ripple. The maximum pressure difference with 240 Pa is 4.4 times lower than for the reference case with 1060 Pa. A decreasing hyporheic exchange is consequently expected for a lower flowrate.

Due to the lower flow velocity the tracer reaches the rippled area after 12 s. After 18 s the main part of the tracer has passed the rippled area. To compare the tracer distribution of the reference case with a flow velocity of 1 m/s after 10 s for this case with 0.5 m/s the tracer distribution after 20 s is compared. Like in the reference case, the tracer is retained between the ripples. A maximum tracer concentration of 12% is determined at the last ripple, similar to the reference case. After 25 s the maximum tracer concentration in the rippled area amounts to 5%. For the reference case even after 18.5 s the concentration was below this value. It takes 74 s until the tracer concentration is lower than 1%. Following this result, it can be deduced that the flow rate is directly related to the residence time if geometry remains the same. Due to lower pressure gradients lower hyporheic exchange is expected, but at the same time the retention of the tracer between the ripples is higher. Which influence is higher for a tracer pulse, still has to be investigated including the porous mediabelow.

5. Conclusions

Ripples in natural stream flows cause disturbances in the water level and enhance turbulent flows which lead to pressure fluctuations and the generation of recirculation zones between the ripples which cause tracer retention and thus has an impact on hyporheic exchange. Pressure distribution can be used to locate an exchange of stream- and groundwater and pressure gradients provide information about the amount of exchange. Previous transport investigations at the surface water groundwater interface, considered the upper boundary of the hyporheic zone mainly with respect to pressure distributions, the exchange of water and the transport within the ground, but they did not consider tracer retention in surface waters. In this study, the retention of a tracer in a rippled streambed was investigated together with pressure fluctuations, flow fields and the generation of recirculation zones between the ripples. Turbulent two-phase open-channel flow and transport processes over idealized ripples with different geometries and two different flow rates were presented. Next to the variation of ripple heights and lengths, the distance between the ripples varied. The effect of ripple spacing was not studied so far. The high-resolution pressure and flow fields can have an impact on the movement and reaction of compounds like oxygen, carbon, nitrogen-species or contaminants (pesticides) in the hyporheic zone.

The model has been validated with data of two experiments as well as with the help of analytical solutions. The flow characteristics and tracer concentration were successfully reproduced with the computational fluid dynamics model OpenFOAM. The LES turbulence model has proven to be most suitable here and it allows to determine eddies for a certain size directly in three-dimensions.

The simulations verified our hypothesis that the ripple geometry (dimension, length and spacing) has significant influence on the hydraulics of the flow, i.e. flow velocity and pressure fluctuations as well as on the tracer spreading and retention. The main tracer transport occurred above the ripples for all cases, where the flow velocity was comparatively high. Between the ripples increased tracer retention was observed due to small velocities and recirculation zones. For decreasing ripple sizes, pressure gradients and tracer retention timewere decreasing. Ripples of a certain size may even cause waves at the water surface due to an undular hydraulic jump with very high pressure gradients. The observed hydraulic jump had a significant effect on the tracer spreading with a significantly reduced retention. The study showed, that turbulence leads to significant changes of residence time for the tracer between the ripples. No recirculations were determined for the highest ripple length to height ratio which led to a fast disappearance of the tracer, whereas the pressure gradient remained at the same size as in the reference case. Consequently, less tracer mass will flow into the subsurface for ripple geometries where no recirculations occur. For increased ripple distances the recirculation zone expands in the flow direction. More tracer mass reaches the interface, but less retention was determined. Observing

lower flow velocities, the pressure gradients decrease whereas the residence time increases due to lower flow velocities. The research showed that the examination of transport processes at the upper boundary including the riverbed morphology is very important for the hyporheic zone. Already small scale ripples influence whether, where, and for how long a tracer is retained in the surface water dead zones and may enter the subsurface.

For a more precise investigation about the change between surface water and the subsurface, the subsurface must be included. This work is currently underway where the surface water and a part of the river bed soil are modelled using an integral approach.

Acknowledgements

Most of the simulations were computed on the supercomputers of Norddeutscher Verbund für Hoch- und Höchstleistungsrechnen in Berlin. The funding provided by the German Research Foundation (DFG) within the Research Training Group ‘Urban Water Interfaces’ in project N6 is gratefully acknowledged.

References

Almeida et al., 1990

G.P. Almeida, D.F.G. Durao, J.P. Simoes, M.V. Heitor**Laser-doppler measurements of fully developed turbulent channel flow**

5th International Symposia on Applications of Laser Techniques to Fluid Mechanics (1990)

Bardini et al., 2012

L. Bardini, F. Boano, M.B. Cardenas, R. Revelli, L. Ridolfi**Nutrient cycling in bedform induced hyporheic zones**

Geochim. Cosmochim. Acta, 84 (2012), pp. 47-61

Boano et al., 2006

F. Boano, C. Camporeale, R. Revelli, L. Ridolfi**Sinuosity-driven hyporheic exchange in meandering rivers**

Geophys. Res. Lett., 33 (18) (2006), p. L18406

Boano et al., 2007

F. Boano, R. Revelli, L. Ridolfi**Bedform-induced hyporheic exchange with unsteady flows**

Adv. Water Resour., 30 (1) (2007), pp. 148-156

Buffington and Tonina, 2009

J.M. Buffington, D. Tonina**Hyporheic exchange in mountain rivers ii: Effects of channel morphology on mechanics, scales, and rates of exchange**

Geogr. Compass, 3 (3) (2009), pp. 1038-1062

Buss et al., 2009

S. Buss, Z. Cai, B. Cardenas, J. Fleckenstein, D. Hannah, K. Heppell, P. Hulme, T. Ibrahim, D.Kaeser, S. Krause, D. Lawler, D. Lerner, J. Mant, I. Malcolm, G. Old, G. Parkin, R. Pickup, G. Pinay, J.Porter, G. Rhodes, A. Richie, J. Riley, A. Robertson, D. Sear, B. Shields, J. Smith, J. Tellam, P. Wood**The Hyporheic Handbook – A Handbook on the Groundwater-surface Water Interface and Hyporheic Zone for Environment Managers**

Environment Agency (2009)

Cardenas, 2008

M.B. Cardenas**The effect of river bend morphology on flow and timescales of surface water groundwater exchange across pointbars**

J. Hydrol., 362 (1–2) (2008), pp. 134-141

Cardenas et al., 2008

M.B. Cardenas, P.L.M. Cook, H. Jiang, P. Traykovski**Constraining denitrification in permeable wave-influenced marine sediment using linked hydrodynamic and biogeochemical modeling**

Earth Planet. Sci. Lett., 275 (1–2) (2008), pp. 127-137

Cardenas and Wilson, 2007

M.B. Cardenas, J.L. Wilson**Dunes, turbulent eddies, and interfacial exchange with permeable sediments**

Water Resour. Res., 43 (2007), p. W08412

Cardenas and Wilson, 2007b

M.B. Cardenas, J.L. Wilson**Hydrodynamics of coupled flow above and below a sediment-water interface with triangular bedforms**

Adv. Water Resour., 30 (3) (2007), pp. 301-313

Chanson and Montes, 1995

H. Chanson, J.S. Montes**Characteristics of undular hydraulic jumps: experimental apparatus and flow patterns**

J. Hydraul. Eng., 121 (2) (1995), pp. 129-144

Chen et al., 2015

X. Chen, M.B. Cardenas, L. Chen**Three-dimensional versus two-dimensional bed form-induced hyporheic exchange**

Water Resour. Res, 51 (2015), pp. 2923-2936

Dahm et al., 1998

C.N. Dahm, N.B. Grimm, P. Marmonier, H.M. Valett, P. Vervier**Nutrient dynamics at the interface between surface waters and groundwaters**

Freshw. Biol., 40 (1998), pp. 427-451

Elliott and Brooks, 1997

A.H. Elliott, N.H. Brooks**Transfer of nonsorbing solutes to a streambed with bed forms: theory**

Water Resour. Res., 33 (1) (1997), pp. 123-136

Fehlman, 1985

H.M. Fehlman**Resistance Components and Velocity Distributions of Open Channel Flows Over Bedforms**

Colorado State University (1985)

(Master's thesis)

Greenshields, 2010

C. Greenshields**Openfoam 1.7.0 released**

(2010)

http://openfoam.org/release/1-7-0/

Harvey and Fuller, 1998

J.W. Harvey, C.C. Fuller**Effect of enhanced manganese oxidation in the hyporheic zone on basin-scale geochemical mass balance**

Water Resour. Res., 34 (4) (1998), pp. 623-636

Hinkelmann, 2005

R. Hinkelmann**Efficient Numerical Methods and Information-Processing Techniques for Modeling Hydro- and Environmental Systems**

Springer-Verlag GmbH (2005)

pp. 48 et seqq

Hirt and Nichols, 1981

C.W. Hirt, B.D. Nichols**Volume of fluid (VOF) method for the dynamics of free boundaries**

J. Comput. Phys., 39 (1) (1981), pp. 201-225

Janssen et al., 2012

F. Janssen, M.B. Cardenas, A.H. Sawyer, T. Dammrich, J. Krietsch, D. de Beer**A comparative experimental and multiphysics computational fluid dynamics study of coupled surface-subsurface flow in bed forms**

Water Resour. Res., 48 (2012), p. W08514

Jirka, 2007

G.H. Jirka**Einführung in die Hydromechanik**

Universitätsverlag Karlsruhe (2007)

pp. 220 et seqq

Kinzelbach, 1992

W. Kinzelbach**Numerische Methoden zur Modellierung des Transports von Schadstoffen im Grundwasser**

Oldenbourg Wissenschaftsv (1992)

ISBN: 978-3486263473

Lane et al., 2002

S.N. Lane, R.J. Hardy, L. Elliott, D.B. Ingham**High-resolution numerical modelling of three-dimensional flows over complex river bed topography**

Hydrol. Process., 16 (2002), pp. 2261-2272

Packman and Brooks, 2001

A.I. Packman, N.H. Brooks**Hyporheic exchange of solutes and colloids with moving bed forms**

Water Resour. Res., 37 (10) (2001), pp. 2591-2605

Revelli et al., 2008

R. Revelli, F. Boano, C. Camporeale, L. Ridolfi**Intrameander hyporheic flow in alluvial rivers**

Water Resour. Res., 44 (12) (2008), p. W12428

Rodrigues et al., 2011

M.A. Rodrigues, L. Pardela, V. Geraldes, J. Santos, H.A. Matos, E.J. Azevedo**Theophylline polymorphs by atomization of supercritical antisolvent induced suspensions**

J. Supercrit. Fluids, 58 (2) (2011), pp. 303-312

Schulze and Thorenz, 2014

L. Schulze, C. Thorenz**The multiphase capabilities of the CFD toolbox openfoam for hydraulic engineering applications**

ICHE 2014, Hamburg. Bundesanstalt für Wasserbau (2014)

Shen and Diplas, 2008

Y. Shen, P. Diplas**Application of two- and three-dimensional computational fluid dynamics models to complex ecological stream flows**

J. Hydrol., 348 (1–2) (2008), pp. 195-214

Stoesser et al., 2008

T. Stoesser, C. Braun, M. García-Villalba, W. Rodi**Turbulence structures in flow over two-dimensional dunes**

J. Hydraul. Eng., 134 (1) (2008), pp. 42-55

Stonedahl et al., 2010

S.H. Stonedahl, J.W. Harvey, A. Wörman, M. Salehin, A.I. Packman**A multiscale model for integrating hyporheic exchange from ripples to meanders**

Water Resour. Res., 46 (12) (2010), p. W12539

Thibodeaux and Boyle, 1987

L.J. Thibodeaux, J.D. Boyle**Bedform-generated convective transport in bottom sediment**

Nature, 325 (1987), pp. 341-343

Tonina and Buffington, 2007

D. Tonina, J.M. Buffington**Hyporheic exchange in gravel bed rivers with pool-riffle morphology: laboratory experiments and three-dimensional modeling**

Water Resour. Res., 43 (2007), p. W01421

Tonina and Buffington, 2009a

D. Tonina, J.M. Buffington**Hyporheic exchange in mountain rivers i: Mechanics and environmental effects**

Geogr. Compass, 3 (2009), pp. 1063-1086

Tonina and Buffington, 2009b

D. Tonina, J.M. Buffington**A three-dimensional model for analyzing the effects of salmon redds on hyporheic exchange and egg pocket habitat**

Can. J. Fish. Aquat. Sci., 66 (12) (2009), pp. 2157-2173

Trauth et al., 2013

N. Trauth, C. Schmidt, U. Maier, M. Vieweg, J.H. Fleckenstein**Coupled 3-d stream flow and hyporheic flow model under varying stream and ambient groundwater flow conditions in a pool-riffle system**

Water Resour. Res., 49 (2013), pp. 5834-5850

Trauth et al., 2014

N. Trauth, C. Schmidt, M. Vieweg, U. Maier, J.H. Fleckenstein**Hyporheic transport and biogeochemical reactions in pool-riffle systems under varying ambient groundwater flow conditions**

J. Geophys. Res. Biogeosci., 119 (2014), pp. 910-928

Trauth et al., 2015

N. Trauth, C. Schmidt, M. Vieweg, S.E. Oswald, J.H. Fleckenstein**Hydraulic controls of in-stream gravel bar hyporheic exchange and reactions**

Water Resour. Res., 51 (2015), pp. 2243-2263

Young et al., 2010

D.F. Young, B.R. Munson, T.H. Okiishi, W.W. Huebsch**A Brief Introduction to Fluid Mechanics**

(5th ed.), John Wiley & Sons Inc (2010)

ISBN 978-0-470-59679-1

Yue et al., 2005

W. Yue, C.-L. Lin, V.C. Patel**Large eddy simulation of turbulent open-channel flow with free surface simulated by level set method**

Phys. Fluids, 17 (2) (2005)

025108–025108